JGR Biogeosciences

RESEARCH ARTICLE
10.1029/2022JG006954

River Corridor Sources Dominate CO_2 Emissions From a Lowland River Network

Lily Kirk[1] **and Matthew J. Cohen**[2]

[1]School of Natural Resources and Environment, University of Florida, Gainesville, FL, USA, [2]School of Forest, Fisheries, and Geomatics Sciences, University of Florida, Gainesville, FL, USA

Key Points:

- River corridors can source most of CO_2 emitted by streams through in-stream metabolic production and lateral transport of riparian soil CO_2
- The dominance of riparian versus upland sources to stream CO_2 emissions depends on lateral drainage flowpath
- Terrestrial uplands yield far less CO_2 to streams than suggested by aquatic mass balance, implying a need to partition lateral C fluxes

Supporting Information:

Supporting Information may be found in the online version of this article.

Correspondence to:

L. Kirk,
lily33@ufl.edu

Citation:

Kirk, L., & Cohen, M. J. (2023). River corridor sources dominate CO_2 emissions from a lowland river network. *Journal of Geophysical Research: Biogeosciences*, *128*, e2022JG006954. https://doi.org/10.1029/2022JG006954

Received 19 APR 2022
Accepted 22 DEC 2022

Author Contributions:

Conceptualization: Lily Kirk, Matthew J. Cohen
Data curation: Lily Kirk
Formal analysis: Lily Kirk, Matthew J. Cohen
Funding acquisition: Matthew J. Cohen
Investigation: Lily Kirk
Methodology: Lily Kirk, Matthew J. Cohen
Project Administration: Lily Kirk
Resources: Matthew J. Cohen
Software: Lily Kirk
Supervision: Matthew J. Cohen
Validation: Lily Kirk
Visualization: Lily Kirk
Writing – original draft: Lily Kirk
Writing – review & editing: Lily Kirk, Matthew J. Cohen

Abstract Rivers and streams are control points for CO_2 emission to the air (fCO_2), with emission rates often exceeding internal metabolism (net ecosystem production, NEP). The difference is usually attributed to CO_2-supersaturated groundwater inputs from upland soil respiration and rock weathering, but this implies a terrestrial-to-aquatic C transfer greater than estimated by terrestrial mass balance. One explanation is that riparian zones—rich in organic and inorganic C but mostly neglected in terrestrial mass balances—contribute disproportionately to fCO_2. To test this hypothesis, we measured fCO_2, NEP, and the lateral CO_2 contributions from both terrestrial uplands (TER) and riparian wetlands (RIP) for seven reaches in a lowland river network in Florida, USA. NEP contributed about half of fCO_2, but the remaining CO_2 emission was generally much larger than measured TER. The relative importance of RIP versus TER varied markedly between contrasting hydrogeologic settings: RIP contributed 49% of fCO_2 where geologic confinement forced lateral drainage through riparian soils, but only 12% where unconfined karst allowed deeper groundwater flowpaths that bypassed riparian zones. On a land area basis, the narrow riparian corridor yielded far more CO_2 than the terrestrial uplands (33.1 vs. 1.4 g-C m^{-2} yr^{-1}), resulting in river corridors (i.e., stream channel plus adjacent wetlands, NEP + RIP) sourcing 87% of fCO_2 to streams. Our findings imply that true terrestrial CO_2 subsidies to streams may be smaller than previously estimated by aquatic mass balance and highlight the importance of explicitly integrating riparian zones into the conceptual model for terrestrial-to-aquatic C transfer.

Plain Language Summary Globally, rivers and streams emit a similar amount of carbon dioxide (CO_2) to the atmosphere as the land retains. To help curb CO_2 emissions that cause climate change, we need to understand what is generating these high rates of stream CO_2 emissions. While biological processes in the stream can generate CO_2, the bulk of stream CO_2 is thought to come from upland soils, carried by run-off from the land to the streams where it off-gases. In this study of seven streams of varying sizes in the same river network, we measured CO_2 fluxes from both the stream and land to better understand where the CO_2 emissions come from. We observed that a large fraction—sometimes all—of the CO_2 delivered to the stream channel from groundwater comes from the wetlands next to the stream. Indeed, about half of CO_2 emissions came from stream organisms consuming organic carbon, and one-third from the thin band of riparian wetlands bordering the stream. Thus, we conclude that the narrow river corridor (the stream plus adjacent wetlands) is the source of 87% of the CO_2 emitted by streams, and that the uplands that comprise most of the land area are a much smaller source than expected.

1. Introduction

Inland waters are control points for continental carbon (C) budgets (Ciais et al., 2008; Cole et al., 2007) with riverine C emissions supported by lateral groundwater inputs enriched in C from terrestrial soils (Siemens, 2003). Globally, terrestrial net ecosystem production (NEP; gross primary production minus total community respiration) is estimated to be 4.5 Pg-C yr^{-1} (Battin et al., 2009), 1.9 Pg-C yr^{-1} of which is transferred laterally from the land to inland water networks (Regnier et al., 2013). An alternate estimate of the terrestrial C subsidy to inland waters is obtained using "active pipe" mass balance in receiving waters, and considers CO_2 emission, downstream transport, and sediment burial (Cole et al., 2007). Estimates of CO_2 outgassing from inland waters—86% from streams and rivers—have recently been revised upward to 2.1 Pg-C yr^{-1} (Raymond et al., 2013) and higher (Drake et al., 2018; Gómez-Gener et al., 2021) globally, which in turn necessitates at least a lateral C transfer of 3.4 Pg-C yr^{-1} from the terrestrial landscape to freshwaters given that they globally export 0.95 Pg-C yr^{-1} to oceans (Regnier et al., 2013), bury 0.6 Pg-C yr^{-1} in sediments (Battin et al., 2009), and photosynthesize 0.3 Pg-C yr^{-1} (Regnier et al., 2013). As the mass accounting of stream CO_2 emission improves, it implies a substantial,

unexplained gap (1.5 Pg-C yr^{-1}) between estimates of terrestrial C lateral export and resulting freshwater emissions. Explaining this discrepancy is integral to resolving the role of inland water networks in the global C cycle.

There are two main pathways—the "reactor" and "chimney"—for terrestrial C to subsidize riverine CO_2 emission, and many recent studies have focused on partitioning the contribution of each (Bernal et al., 2022; Hotchkiss et al., 2015; Lupon et al., 2019; Rasilo et al., 2017; Saccardi & Winnick, 2021). The "reactor" pathway arises from lateral transport of terrestrially derived organic matter, which fuels in-stream ecosystem respiration (ER), producing net CO_2 in the stream that then off-gases (Cole & Caraco, 2001; Mayorga et al., 2005). The "chimney" pathway, in contrast, arises from in-stream emission of inorganic carbon derived from soil respiration and/or mineral weathering: Surface and especially subsurface flowpaths deliver water supersaturated with CO_2 to streams, which rapidly degasses as stream waters equilibrate with the atmosphere (Duvert et al., 2019; Johnson et al., 2008). The amount of CO_2 derived from organic matter subsidies (i.e., the reactor pathway) is estimated using stream net ecosystem production (NEP), defined as the difference between gross primary production (GPP) which consumes CO_2 and aerobic ER which produces it (anaerobic respiration is typically neglected in NEP). The amount of CO_2 derived from inorganic subsidies (i.e., the chimney pathway) is estimated as the difference between CO_2 emission and NEP. Unlike the reactor pathway, the chimney pathway is typically measured only by difference, so these fluxes and their provenance remain poorly constrained, despite recognizing the need to improve direct estimates (Johnson et al., 2006).

Existing conceptual models of C mass transfer separate the landscape into terrestrial and aquatic components, largely ignoring ecotonal riparian wetlands that exist at their interface. Riparian wetlands comprise 7% of global wetland area (Abril & Borges, 2019), are ubiquitous and common to all latitudes (boreal, temperate, tropical) and network positions including headwaters (Leith et al., 2015), and exert important controls on flowing waters even when connectivity is sporadic (Junk, 1989; Raymond et al., 2016). Crucially, wetlands are structurally and functionally different from both freshwater and terrestrial environments, with distinctive plant communities (Naiman & Décamps, 1997) and persistent hydric conditions (Burt et al., 2002) that facilitate high rates of primary production, and strong redox gradients that enable biogeochemical reactivity (Hedin et al., 1998; Vidon et al., 2010) and organic matter accumulation (Mitra et al., 2005). Prolonged saturated conditions inhibit soil ventilation which limits losses of CO_2 generated from both aerobic and anaerobic respiration to the air. Because groundwater often flows at shallow depths through riparian zones before reaching the river channel, these wetland areas can exert a disproportionate influence on stream chemistry (Hooper et al., 1998). Groundwater transport through riparian zones substantially increases concentrations of dissolved organic carbon (DOC) (Chestnut & McDowell, 2000), with source apportionment studies suggesting stream DOC is derived primarily from the riparian zone not uplands (Ledesma et al., 2018; Mayorga et al., 2005). The combination of soils with large organic matter stocks and reduced ventilation results in groundwater CO_2 concentrations that are greatly elevated and create a "wetland CO_2 pump" capable of influencing C mass flux toward streams and rivers (Abril & Borges, 2019). Indeed, Abril and Borges (2019) argue that inclusion of riparian wetlands as a C source distinct from true upland terrestrial areas is crucial to enumerating the "active pipe" of inland waters, and other authors have acknowledged the "largely unknown and yet potentially large fluxes from floodplains" (Drake et al., 2018; Regnier et al., 2022).

The importance of riparian wetlands as a source of lateral CO_2 inputs ultimately depends on the dominant flowpath(s) of water to the stream (e.g., Dinsmore & Billett, 2008). Flowpaths range from overland flow that interacts minimally with soils to shallow groundwater flow through soil layers with high organic matter respiration rates, to deeper groundwater flows through mineral soil or bedrock where respiration rates are likely to be far lower (Fisher et al., 2004). For river systems interacting with large aquifers, groundwater pathways may include deep regional—that is, not just local—flow lines (Dahl et al., 2007). The relative importance of these distinct flowpaths vary over space and time (Liu et al., 2022; Mulholland, 1993) and depends on climate, lithology, geomorphology, vegetation, and soil characteristics (Fisher et al., 2004), factors which, in turn, also control the chemistry of lateral water inputs (Chen et al., 1984; Ohrui & Mitchell, 1999). For example, recent work shows how stream riparian buffers variably lower nitrate from upland runoff depending on whether the water flows through (Maître et al., 2003) or bypasses (Devito et al., 2000) the riparian zone (Cirmo & McDonnell, 1997; Puckett et al., 2002). While it remains speculative, the riparian contribution to lateral organic matter and CO_2 inputs is expected to be equally dependent on flowpath prominence (Figure 1).

Strong and persistent bi-directional coupling between streams and adjacent riparian wetlands has prompted focus on the river corridor—that is, the wetted channel plus the hyporheic and riparian zones—as a single operational unit (Fisher et al., 1998, and more recently, Harvey & Gooseff, 2015). The overarching hypothesis of this work

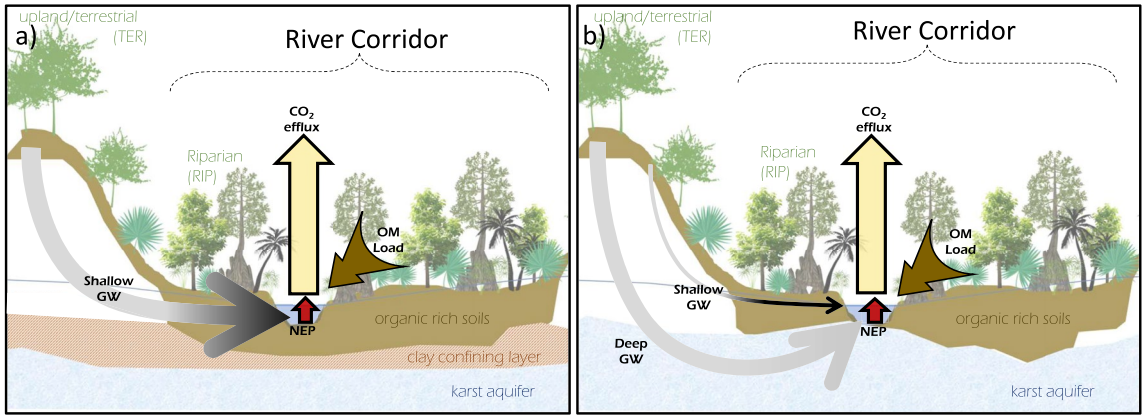

Figure 1. Conceptual diagram illustrating the influence of landscape hydrogeology on lateral CO_2 sources. (a) The presence of an impermeable confining layer forces water draining the uplands (i.e., the terrestrial system) to flow through riparian soils and entrain CO_2. (b) In the absence of a confining layer, water draining the terrestrial uplands enters a deep aquifer and largely bypasses riparian soils. Groundwater arrow color (gray to black) indicates CO_2 concentration, and arrow size indicates CO_2 mass flux. River corridor (i.e., stream and adjacent wetlands) contribute CO_2 via both allochthonous organic matter inputs that dominates net ecosystem production (NEP = GPP + ER) as well as accumulation of dissolved CO_2 along lateral input flowpaths that interact with organic matter rich soils in riparian wetlands.

is that the river corridor is the primary source of CO_2 evaded from the stream to the atmosphere, providing the C as both DOC and DIC that amplify both the reactor and chimney pathways. The conceptual framework used explicitly includes riparian zones in the CO_2 mass balance of landscapes (Figure 1). From this framework we sought to partition lateral CO_2 transfer to streams into fluxes originating from the terrestrial landscape (TER) versus fluxes derived from passage through the riparian zone (RIP), and thus better constrain the spatial contributions of CO_2 contributing to the chimney pathway (Raymond et al., 2013). We conducted our study in the Santa Fe River of north-central Florida, USA, where we had the opportunity to observe these fluxes under contrasting groundwater flowpaths (Figure 1). We predicted that lateral CO_2 inputs are dominated by RIP sources especially when groundwater flowpaths are shallow (but not exclusively so), and that, by extension, the C subsidy to streams attributed to terrestrial environments (TER) is smaller than previously assumed, and better aligned with estimates from terrestrial C mass balance. Because the subtropics are particularly important for atmospheric CO_2 efflux compared to higher latitudes (Lauerwald et al., 2015), and because lowlands amplify the spatial extent of riparian wetland area, partitioning sources of CO_2 in this river network is relevant to understanding global C cycling.

2. Materials and Methods

2.1. Study Sites

The Santa Fe River (SF), a major tributary of the Suwannee River, is 121 km long and drains 3,585 km^2 of the southeastern coastal plain in Florida, USA. Like many of the rivers in the coastal plain, this low gradient network (mean bed slope = 0.74 m/km; Hensley et al., 2019) is bordered along its length by extensive riparian forests (widths of 50–1,400 m) dominated by cypress (*Taxodium distichum*) and hardwoods (Florida Natural Areas Inventory, 1990). The climate is warm and humid with mean annual temperature of 21°C and mean annual precipitation of 1,248 mm yr^{-1} (2008–2018, Florida Automated Weather Network). Despite the abundant rainfall, water yields across north Florida are relatively low (100–200 mm yr^{-1}) because of high rates of evapotranspiration (900–1,100 mm yr^{-1}; Douglas et al., 2009).

We selected seven stream reaches that represent second (DRAIN), third (SF700, SF1000), fourth (SF1500), and fifth order (SF2500, SF2800) network positions and were co-located with USGS gauging stations (waterdata.usgs.gov/nwis for site descriptions; site nomenclature is based on the last four digits of the stations' identification number). Our stream reaches span stark differences in landscape geology (Figure S1c). The SF basin is entirely underlain by the Upper Floridan aquifer, but connectivity between surface waters and this deep aquifer is spatially controlled by the presence or absence of the Miocene Hawthorne Group, a thick low permeability clay layer that confines vertical water movement. In the upper SF basin, the confining unit results in a shallow perched aquifer that creates numerous surface water features (streams, lakes, and wetlands). Interactions with wetlands, which comprise 9% of the upper basin area, make sites in the upper SF (DRAIN, SF700, SF1000, SF1500) blackwater streams, with low pH and high DOC concentrations. In the lower watershed, erosion of the

Hawthorne Group has exposed the carbonate deep aquifer, favoring rapid vertical recharge resulting in dramatically reduced surface water features; wetlands comprise <2% of the lower basin area (Figure S1c). Along these lower basin reaches (ICHE, SF2500, SF2800) the SF receives discrete lateral inputs from artesian Floridian aquifer springs. This water is clear, alkaline and thermally stable (Jin et al., 2015; Khadka et al., 2014), and dominates total discharge at low streamflow. At higher flow, discharge from the far more temporally dynamic upper basin dominates discharge, creating blackwater conditions throughout the network (Hensley et al., 2019) and even in the lower ICHE, a spring-fed tributary to the SF. Gaining conditions persist along most of the SF except at the transition between confined and unconfined areas, where the river flows into a large sinkhole, re-emerging 8 km downstream after passing through a network of subsurface karst conduits. Although land use and vegetation cover differ between the upper (mostly pine forests) and lower basins (mostly pasture), the entire watershed remains relatively undeveloped, with 11% urban land cover, and >60% cover by forest and wetlands.

Differences in water clarity and stream size result in substantial heterogeneity in stream metabolism (Kirk et al., 2020): High color and canopy cover in the upper river reaches result in GPP only slightly above zero, while the clear, wide, spring-fed rivers have high GPP driven by dense aquatic macrophyte beds and attached algal communities (Odum, 1957). The lower SF exhibits marked variation in GPP in response to the time-varying blend of dark and clear water. ER is high throughout the network, but covaries with GPP such that the highest rates are in spring-fed rivers where GPP/ER is closest to 1 (Odum, 1957).

2.2. Data Collection, Calculations, and Analysis

Direct measurements of lateral inputs of water and solutes are necessary to constrain and partition terrestrial-to-aquatic carbon transfers. To test our hypothesis, we measured stream CO_2 emission, in-stream aerobic metabolism (GPP and ER), lateral water fluxes (q_L), and groundwater pCO_2 at both the stream edge (RIP + TER) and uphill from the river corridor edge (TER only). Stream reaches were defined as $0.7u/k_{600}$ upstream of the gage using average values, where u is stream velocity in m d^{-1} (Lamberti & Hauer, 2017) and k_{600} is a normalized gas transfer coefficient in d^{-1} (see Methods 2.2.1), to represent the dominant stream footprint for signal genesis based on gas exchange, acknowledging that the CO_2 footprint may be longer due to ionization into bicarbonate that does not degas (Stets et al., 2017). We measured all fluxes at most reaches for 3–7 months in 2019, but due to sensor failure, we have limited data from both SF700 (January–February) and SF2800 (September) (Table 1). We propagated uncertainties in key variables (e.g., reaeration coefficients, groundwater CO_2 concentrations, and lateral inflow rates) through the mass balance calculations using Monte Carlo simulations (250 simulations per day per site) to determine 2.5%, 25%, 75%, and 97.5% credible intervals for CO_2 fluxes (Text S3 in Supporting Information S1). Additionally, we performed Monte Carlo simulations (10,000 simulations) using average site conditions that captured maximum uncertainties due to methodological bias (Text S3 in Supporting Information S1). Data and statistical analyses were conducted using Excel (version 2209) and R (version 3.6.2).

2.2.1. Stream CO_2 Emission

CO_2 emission (fCO_2, g-C m^2 d^{-1}) from stream to atmosphere was based on Fick's Law:

$$fCO_2 = k_{CO_2}(pCO_{2,\text{stream}} - pCO_{2,\text{atm}}) \times K_H \times \frac{1\,\text{atm}}{10^6\,\text{ppm}} \times \frac{12\,\text{g C}}{1\,\text{mol C}} \times \frac{1000\,\text{L}}{1\,\text{m}^3} \times z \quad (1)$$

where k_{CO2} is the reaeration coefficient (d^{-1}), $pCO_{2,\text{stream}}$ is the partial pressure of CO_2 in air equilibrated with the stream water (ppm), $pCO_{2,\text{atm}}$ is the partial pressure of CO_2 in air (assumed 400 ppm), K_H is the temperature dependent Henry's constant (mol L^{-1} atm^{-1}) corrected using the Van't Hoff equation (Smith & Harvey, 2007), and z is mean stream depth (m). Stream pCO_2 was measured every 15 min with a submersible infrared gas analyzer (0–20,000 or 0–30,000 ppm range, Eosense eosGP, Nova Scotia, Canada) connected to a datalogger (Campbell Scientific CR1000, Utah, USA). Factory calibration was checked against air before every use and against known CO_2 gas concentrations annually. We post-corrected pCO_2 measurements based on pressures experienced by the submerged sensor using a pressure transducer (Onset HOBO U20, Bourne, Massachusetts, USA).

For each river reach, k_{600} was estimated from channel hydraulics using the mean of Equations 1–7 in Raymond et al. (2012), as well as directly measured in unanchored floating domes at each site. The floating dome consisted of a clear, rectangular storage container (area = 0.084 m^2) overturned on the water surface, supported by flotation collars that penetrated 5 cm into the water, yielding a constant headspace volume of 15.5 L. CO_2 was injected into

Table 1
Site Characteristics Between the Upper (Dark Gray) and Lower (Light Gray) Santa Fe River Network for the Entire Period of Record

	Drain	SF700	SF1000	SF1500	ICHE	SF2500	SF2800
USGS site code	--	02320700	02321000	02321500	02322700	02322500	02322800
Median discharge ($m^3\ s^{-1}$)	0.02 ± 0.16	0.5 ± 1.3	0.4 ± 3.6	1.8 ± 11.7	9.6 ± 0.9	38.3 ± 13.7	50.9 ± 16.1
Median baseflow ($m^3\ s^{-1}$)	0.01 ± 0.05	0.2 ± 0.6	0.3 ± 1.7	0.8 ± 4.4	9.4 ± 0.8	36.1 ± 8.5	49.0 ± 8.9
Width (m)	1 ± 1	6 ± 2	6 ± 8	24 ± 19	42 ± 1	49 ± 3	46 ± 2
Depth (m)	0.4 ± 0.2	0.5 ± 0.3	1.0 ± 0.2	1.6 ± 0.5	1.0 ± 0.0	1.8 ± 0.1	3.6 ± 0.0
Velocity ($m\ s^{-1}$)	0.06 ± 0.05	0.15 ± 0.08	0.16 ± 0.04	0.31 ± 0.05	0.45 ± 0.01	0.42 ± 0.07	0.32 ± 0.07
Water temp. (°C)	20.1 ± 4.3	17.4 ± 3.8	21.3 ± 5.1	21.0 ± 5.1	21.8 ± 1.2	22.1 ± 2.1	20.6 ± 2.7
DO ($mg\ L^{-1}$)	6.2 ± 1.3	7.6 ± 0.9	5.1 ± 1.8	6.3 ± 1.4	5.2 ± 0.5	5.0 ± 0.7	5.9 ± 1.0
Alkalinity ($meq\ L^{-1}$)		0.7 ± 0.6	0.9 ± 0.4	0.6 ± 0.3	2.9 ± 0.1	2.9 ± 0.4	2.8 ± 0.3
pH	4.33 ± 0.44	5.09 ± 0.45	5.91 ± 0.50	6.14 ± 0.7	7.15 ± 0.27	7.06 ± 0.95	7.67 ± 0.41
Stream pCO_2 (ppm)	7,500 ± 2,100	3,400 ± 800	2,900 ± 1,100	4,300 ± 1,200	2,500 ± 400	6,000 ± 700	5,000 ± 800
Upland groundwater pCO_2 (ppm)	--	10,300	--	10,900	7100 ± 500	8,600	13,000
Riparian groundwater pCO_2 (ppm)	50,100 ± 17,000	42,300	73,500	61,400	21,600 ± 9,000	12,700	21,300
k_{600} (d^{-1})	6.4 ± 2.7	4.1 ± 1.6	2.8 ± 0.8	2.3 ± 0.6	2.6	1.5 ± 0.4	0.7
Positive GPP ($g\text{-}O_2\ m^{-2}\ d^{-1}$)	−0.0 ± 0.4	−0.0 ± 0.1	−0.2 ± 0.5	0.5 ± 0.8	7.8 ± 3.5	6.5 ± 7.7	1.4 ± 2.2
Positive ER ($g\text{-}O_2\ m^{-2}\ d^{-1}$)	6.6 ± 4.3	4.2 ± 3.2	10.2 ± 2.6	11.2 ± 3.0	7.0 ± 3.4	6.0 ± 5.6	9.0 ± 2.5
# days	146	52	96	205	85	108	3

Note. Unless otherwise specified, means of daily values are reported with one standard deviation. Alkalinity data from Khadka et al. (2014). The number of days in 2019 where we were able to apply the full CO_2 mass balance is given in the last row.

the headspace, and its concentration was measured every minute in the dome headspace and in the river water below the dome as the dome floated downstream. The slope between concentration and time defined the molar CO_2 flux from dome to water, from which we estimated k_{600} using Khadka et al. (2014). We were able to capture a range of flow conditions with the floating dome measurements, which agreed well with k_{600} from Raymond equations. Both estimates of k_{600} were used as priors for sites where streamMetabolizer was used to model metabolism (see below) and estimate a daily k_{600}. Specifics about the priors and correlations with ecosystem respiration are found in the supplement of Kirk et al. (2020). k_{CO2} was obtained from k_{600}, using stream temperature and Schmidt number scaling (Raymond et al., 2012).

2.2.2. Stream Metabolism

Net ecosystem production (*NEP*, $g\text{-}C\ m^{-2}\ d^{-1}$) is

$$\mathrm{NEP} = (\mathrm{GPP} + \mathrm{ER}) \times \frac{12\mathrm{g\,C}}{32\mathrm{g\,O_2}} \tag{2}$$

where *GPP* is daily gross primary production ($g\text{-}O_2\ m^{-2}\ d^{-1}$) and *ER* is daily ecosystem respiration ($g\text{-}O_2\ m^{-2}\ d^{-1}$, a negative value). For all sites except the spring-fed ICHE, we determined GPP and ER using the single-station open channel method (Odum, 1956) implemented using inverse modeling in streamMetabolizer (Appling, Hall, et al., 2018; Appling, Read, et al., 2018; https://github.com/USGS-R/streamMetabolizer), and assumed photosynthetic and respiratory quotients (i.e., molar ratio of $C:O_2$) of 1.0. StreamMetabolizer chooses combinations of daily GPP, daily ecosystem respiration, and reaeration coefficient (k_{600}) to optimize model alignment with observed sub-daily variation in dissolved oxygen (DO). Stream DO was measured every 15 min with an optical sensor (Onset HOBO U-26, Bourne, Massachusetts, USA) which also measured temperature. Sensors were cleaned monthly and calibrated at least yearly. To estimate metabolism at ICHE, we used a two-station method (Odum, 1956) following Hensley et al. (2015) to account for the discontinuity (springs) at the upstream end of the reach. Details about two-station stream metabolism modeling can be found in Kirk et al. (2020).

Given the magnitude of lateral inflows (q_L, see below) and likely differences between stream and lateral inflow DO, a groundwater correction for metabolism was not necessary at the upper river reaches nor at SF2800 based

on the recommendations of Hall and Tank (2005) (Text S4 in Supporting Information S1). At ICHE, almost all the groundwater comes from springs in the upper third of the river, so the upstream boundary DO was adjusted to reflect the average of these discrete spring inputs. However, at SF2500 where springs are evenly distributed along the entire reach, a groundwater correction was done on a daily time-step based on Hall and Tank (2005):

$$\mathrm{NEP_{correct}} = \mathrm{NEP_{uncorrect}} - \left(\mathrm{DO_{springs}} - \mathrm{DO_{stream}}\right)\frac{q_L}{w} \times \frac{1000\,\mathrm{L}}{1\,\mathrm{m^3}} \times \frac{1\,\mathrm{g\,O_2}}{1000\,\mathrm{mg\,O_2}} \times \frac{12\mathrm{g\,C}}{32\mathrm{g\,O_2}} \times \frac{86400\,\mathrm{s}}{1\,\mathrm{d}} \quad (3)$$

$$\mathrm{ER_{correct}} = \mathrm{ER_{uncorrect}} - \left(\mathrm{DO_{springs}} - \mathrm{DO_{stream,night}}\right)\frac{q_L}{w} \times \frac{1000\,\mathrm{L}}{1\,\mathrm{m^3}} \times \frac{1\,\mathrm{g\,O_2}}{1000\,\mathrm{mg\,O_2}} \times \frac{12\mathrm{g\,C}}{32\mathrm{g\,O_2}} \times \frac{86400\,\mathrm{s}}{1\,\mathrm{d}} \quad (4)$$

$$\mathrm{GPP_{correct}} = \mathrm{NEP_{correct}} - \mathrm{ER_{correct}} \quad (5)$$

where DO_{stream} is the mean daily river DO concentration (mg L^{-1}), $DO_{stream,night}$ is the night-time mean DO concentration in the river, $DO_{springs}$ is the average DO concentration of the major springs of the reach, w is stream width (m), and the subscripts "correct" and "uncorrect" stand for corrected and uncorrected fluxes, respectively.

2.2.3. Lateral CO_2 Fluxes

2.2.3.1. Water Fluxes

All sites except DRAIN were co-located with US Geological Survey (USGS) discharge gages. At DRAIN, a rating curve was developed from 5 years of monthly flow measurements and continuous stage (Hensley et al., 2020). We measured mean width and depth on 4–11 transects in each of the seven reaches and used these empirical measurements to adjust hydraulic geometry equations (Leopold & Maddock, 1953) derived from USGS data at the most downstream transect. In 2019, discharge in the entire SF network was 18% higher than the 10-year average (50.6 $m^3\ s^{-1}$ at SF2800, 2010–2019, USGS).

We estimated lateral water inflows (q_L) using mass balance approaches appropriate for larger spatial measurement scales (see Kalbus et al., 2006). To avoid overestimating lateral inputs of CO_2 during periods of overland flow (i.e., at high discharge) we focus our analysis of q_L on baseflow (Q_{base}) instead of total stream discharge (Kalbus et al., 2006). Hydrograph separation into high-frequency surface runoff variation and low-frequency baseflow variation was performed using a recursive digital filter (Nathan & McMahon, 1990) in the EcoHydRology open-source software package (version 0.4.12.1) in R (Fuka et al., 2018). The α filter parameter was determined empirically at each site as the regressed slope of discharge on day i+1 plotted against discharge on day i during the baseflow portion of the hydrograph recession (Bosch et al., 2017; Eckhardt, 2008). The filter was passed twice over the streamflow record.

We calculated q_L in two ways. First, we used the upslope contributing area (UCA) in the manner of Leach et al. (2017). Digital elevation model (DEM) data came from Mapzen Terrain Tiles, whose underlying data is a mix of open data sets including the USGS National Elevation Data set, and whose advantage is higher resolution (7–10 m at the latitude of our sites). Mapzen Terrain Tiles were accessed with the *elevatr* package (version 0.4.2) in R. DEM data were processed with the Hydrology toolset in ArcGIS Pro 3.0.0 (ESRI, Redlands, CA). First, the DEM was filled to remove closed depressions. Then for each reach, we regressed flow accumulated versus distance upstream of the gage, with the slope indicating the proportional flow accumulation per unit length (ΔUCA, m^{-1}). Only river segments without major tributaries were considered for our regressions. Multiplying by stream baseflow (Q_{base}) gives lateral inflow per unit length (q_L; $m^3\ s^{-1}\ m^{-1}$):

$$q_L = \Delta\mathrm{UCA} \times Q_{\mathrm{base}} \quad (6)$$

Assuming flow accumulation is proportional to drainage area is likely valid in the upper SF sites, but less so in the karstic lower watershed where discrete aquifer inflows (i.e., springs) dominate the lateral input process.

Our second lateral inflow method, the delta Q method, was based on changes in stream discharge between USGS gages (ΔQ_{base}):

$$q_L = \frac{\Delta Q_{\mathrm{base}}}{\Delta x} \quad (7)$$

where Δx is the downstream distance between gages (m). We used the gages corresponding to study sites as well as other gages intermittently monitored by USGS, but where the local water managers have modeled discharge

from continuously monitored stations (e.g., 02320849 and 02320815; Suwanee River Water Management District, 2007). The thalweg distance between gages from Google Earth aerial imagery was used to estimate Δx. To control for overestimation of q_L due to discrete tributary inputs, we estimated and subtracted flow accumulation from all mapped tributaries where discharge was greater than 0.5 $m^3\ s^{-1}$.

In the lower SF network, lateral inflow from the landscape (TER) either flows through the riparian corridor on the way to the river channel (i.e., similar to our conceptual model in the upper SF) or flows below the riparian corridor, entering the river channel at discrete spring vents. To estimate streamflow accumulation from the aquifer at the SF2500 reach ($q_{L,\text{aquifer}}$; 0.0019 $m^3\ s^{-1}\ m^{-1}$), we used longitudinal flow estimates (Suwanee River Water Management District, 2019) for 10 km of the reach that includes 28 named springs. Assuming spring inputs are relatively constant, the difference between river flow accumulation between gages and $q_{L,\text{aquifer}}$ is lateral inflow that passes through the riparian zone (q_L):

$$q_L = \frac{\Delta Q_{\text{base}}}{\Delta x} - q_{L,\text{aquifer}} \tag{8}$$

Since the SF2800 reach has far fewer and much smaller springs, we determined q_L using Equation 7, recognizing this is likely to be an overestimate.

At spring-fed ICHE, neither UCA or delta Q methods were used to determine q_L since flow accumulation is almost entirely from the aquifer at discrete springs. Previous studies using ion composition, fluorescent dyes, and radon mass balances estimate 12%–16% of ICHE flow did not originate from the large named springs (Khadka et al., 2017; Kurz et al., 2015) and 23% of this unaccounted flow originated from diffuse groundwater inflows (the remainder originates from small unnamed springs; Kurz et al., 2015). Therefore, we estimated time-varying q_L as:

$$q_L = \frac{Q_{\text{base}} \times 0.16 \times 0.23}{x} \tag{9}$$

where x is reach length (m). The rest of Q_{base} was attributed to aquifer inputs.

To validate UCA and delta Q estimates, diffuse groundwater flow was also calculated using Darcy's Law at DRAIN and ICHE (Text S1 in Supporting Information S1). We used the mean q_L across all methods, except at SF2500 and SF2800 where we only used the delta Q method. We calculated proportional groundwater input rates (k_{gw}) as q_L divided by baseflow discharge (Q_{base}).

2.2.3.2. Groundwater CO_2 Concentrations

We measured pCO_2 in riparian well water at DRAIN and ICHE (representing the lateral water source end members) monthly using Eosense dissolved CO_2 sensors (range of headspace concentrations = 0–120,000 ppm). Wells were screened between 0.5 and 1.5 m below ground, capped between measurements, and were purged with three well volumes prior to measurements. To expedite sensor equilibration time to within an hour for logistical reasons, we initially filled the well headspace with air supersaturated with CO_2 before deploying the sensors. Sensors were deployed until headspace pCO_2 equilibrated with the groundwater.

We took a synoptic groundwater pCO_2 measurements in an augered hole at each of the remaining sites, with holes situated to capture pCO_2 of riparian and terrestrial groundwater (Figures S1a, S1b). Testing at DRAIN showed that pCO_2 in augered holes did not significantly differ from pCO_2 measured in wells ($t = 0.51$, df = 2.23, $p = 0.66$). Since groundwater pCO_2 ($pCO_{2,\text{gw}}$) varied far less than q_L (Figure S2) and lateral CO_2 mass fluxes were not nearly as sensitive to uncertainty in $pCO_{2,\text{gw}}$ compared with uncertainty in q_L (Text S3 in Supporting Information S1), these synoptic $pCO_{2,\text{gw}}$ values are likely sufficient for estimating lateral CO_2 mass fluxes, despite not capturing temporal variation. Our upland $pCO_{2,\text{gw}}$ values are derived solely from synoptic measurements, but appear representative of true upland values because they are (a) remarkably consistent across all sites (CV = 0.17), (b) slightly higher than spring vent (i.e., aquifer) pCO_2 (10,703 vs. 7,115 ppm), and (c) were equilibrated for the same duration as riparian sensors despite far lower concentrations.

2.2.3.3. Lateral CO_2 Fluxes

Lateral CO_2 mass flux (LI, g-C $m^2\ d^{-1}$ on a stream benthic area basis) was calculated as:

$$\text{LI} = q_L \times pCO_{2,\text{gw}} \times K_H \times \frac{1\ \text{atm}}{10^6\ \text{ppm}} \times \frac{12\ \text{g C}}{1\ \text{mol C}} \times \frac{1000\ \text{L}}{1\ \text{m}^3} \times \frac{86400\ \text{s}}{1\ \text{d}} \times \frac{1}{w} \tag{10}$$

We used upland $pCO_{2,gw}$ to determine LI entering the riparian zone, which is synonymous with upland CO_2 mass flux (*TER*). We used riparian $pCO_{2,gw}$ to determine LI entering the river channel ($LI_{channel}$). The riparian corridor contribution to the river (*RIP*) was

$$\mathrm{RIP} = \mathrm{LI}_{\mathrm{channel}} - \mathrm{TER} \tag{11}$$

Where applicable, the aquifer contribution (*aquifer*, g-C m^{-2} d^{-1}) used Equation 10 with $q_{L,\mathrm{aquifer}}$ and upland $pCO_{2,gw}$.

2.2.4. CO_2 Mass Balance

The full reach-scale CO_2 mass balance is:

$$f\mathrm{CO}_2 + \mathrm{NEP} + \mathrm{export} + \mathrm{other} = \mathrm{RIP} + \mathrm{TER} + \mathrm{input} + \mathrm{aquifer} \tag{12}$$

where *export* is downstream export of CO_2 out of the reach and *input* is CO_2 input from upstream. In the upper river network with confined aquifer, there were no deep aquifer inputs and we could assume CO_2 mass did not change longitudinally (i.e., *export* = *input*) simplifying the mass balance to:

$$f\mathrm{CO}_2 + \mathrm{NEP} + \mathrm{other} = \mathrm{RIP} + \mathrm{TER} \tag{13}$$

In the lower river, aquifer inputs can greatly exceed water contributions from upstream reaches. Since CO_2 in aquifer water is ultimately sourced from the terrestrial springshed, we subsumed the discrete inputs (i.e., *aquifer* + *input* - *export*) as part of *TER*, thus also simplifying the mass balance to Equation 13 and allowing CO_2 flux comparisons directly between upper and lower river reaches. We assumed stream CO_2 mass did not change from 1 day to another, corroborated by remarkably stable daily mean stream CO_2 observations. While carbonate buffering could be a substantial flux in this mass balance for lower SF reaches, a very limited period of record of accurate stream pH measurements was available; we therefore chose not quantify carbonate buffering directly, but rather subsumed it into the "other" flux. For the CO_2 mass balance, the signs of the fluxes were adjusted so that positive and negative fluxes indicated CO_2 entering and leaving the water column, respectively.

All daily fluxes were reported on a benthic area basis. However, we also scaled the lateral transfer of CO_2 from *RIP* (g C m^{-2} d^{-1}) and *TER* to the areal footprint of the riparian corridor (RIP_{yield}; g m^{-2} yr^{-1}) and terrestrial uplands (TER_{yield}), respectively, to calculate C yields from these different contributing land areas:

$$\mathrm{RIP}_{\mathrm{yield}} = \mathrm{RIP} \times \frac{w}{W_{\mathrm{rip}}} \times \frac{365\,\mathrm{d}}{1\,\mathrm{y}} \tag{14}$$

$$\mathrm{TER}_{\mathrm{yield}} = \mathrm{TER} \times \frac{w}{w_{\mathrm{up}} - w_{\mathrm{rip}}} \times \frac{365\,\mathrm{d}}{1\,\mathrm{y}} \tag{15}$$

where W_{up} and W_{rip} are the mean widths (m) of the upland and riparian watersheds, respectively, excluding stream width. W_{up} was calculated as ΔUCA divided by stream reach length. Replicate riparian widths (n = 10 per reach) evenly spaced along the study reach were measured in ArcMap using the National Wetlands Inventory layer and averaged to estimate W_{rip}.

3. Results

Variation in hydrology and water chemistry across sites was substantial, reinforcing the core controls of network position and geologic context on river corridor function. Streamflow was far more dynamic at upper SF sites (CV_Q = 7.1) than lower sites (CV_Q = 0.3). As such, baseflow separation reduced median Q_{base} discharges substantially more in the upper sites (mean = 45%) than lower sites (4% lower median Q_{base} vs. median Q in Table 1). Across all sites except the spring-fed ICHE, baseflow separation reduced temporal variation in flow, but was for more pronounced in the upper sites (mean = 60%) than the lower sites (mean = 41%).

There was broad agreement among methods used to estimate q_L and k_{gw} at all sites except ICHE (Figure 2). SF700, SF1000, and SF1500 showed no significant difference between q_L using UCA and delta Q methods. At DRAIN, point measurements of q_L in the riparian wells agreed with delta Q estimates, but not with estimates using UCA. At ICHE, q_L calculated from well hydraulic gradients was an order of magnitude smaller than q_L

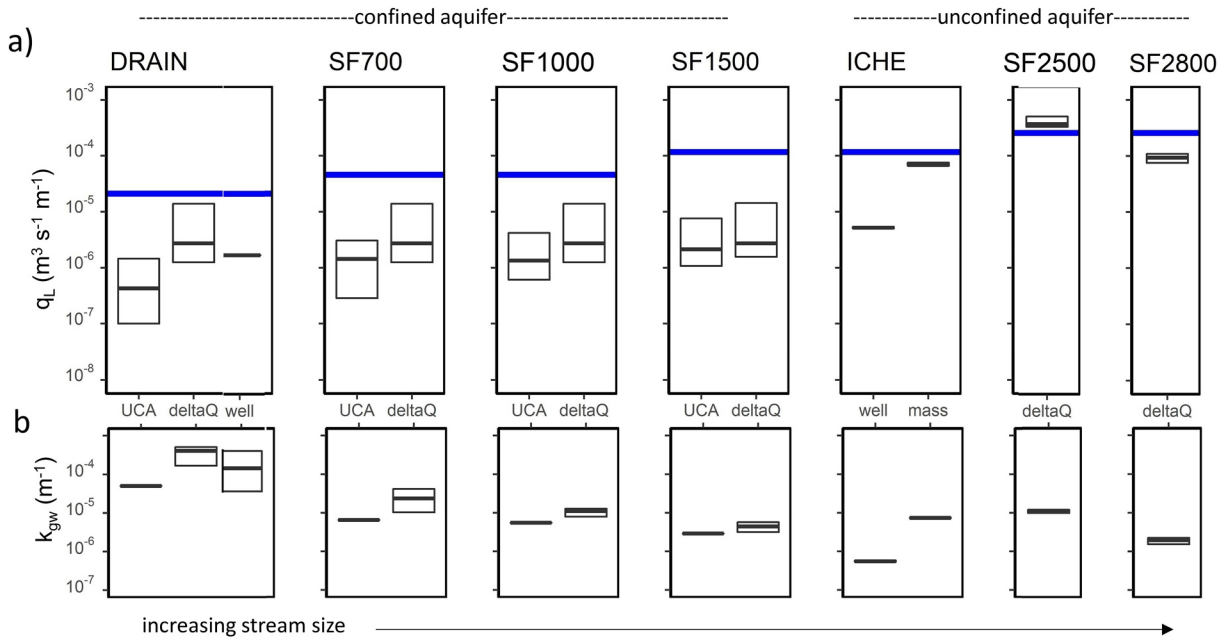

Figure 2. Comparisons of (a) groundwater inflow (q_L) and (b) proportional groundwater input rate (k_{gw}) measured and estimated with various methods, including upslope contributing area (UCA), longitudinal change in discharge (delta *Q*), Darcy's law (well), and ion/dye/radon mass balance (mass). Boxes represent the 25–75th percentiles. Blue lines represent q_L predictions from Hotchkiss et al. (2015) if all excess CO_2 was attributed to terrestrial upland lateral inputs given groundwater pCO_2 = 13,000 ppm, representing the upper bound of upland $pCO_{2,gw}$ measured in this study.

estimated from dye, ion, or radon mass balances in previous studies (Khadka et al., 2017; Kurz et al., 2015), so propagating an average q_L across the various methods to calculate lateral CO_2 fluxes may have led to significant underestimates. We found SF2500 and SF2800 q_L comparable to UCA calculations for a stretch of river between these two reaches with no spring inputs ($q_L \sim 2.6 \times 10^{-4}$).

All reaches were consistently supersaturated with CO_2 (mean pCO_2 = 2,500–7,500 ppm). While stream pCO_2 did not differ significantly between upper and lower SF sites (4,500 ± 2,000 vs. 4,500 ± 1,800, respectively; $t = 0.40$, df = 4.80, $p = 0.97$), riparian groundwater pCO_2 was significantly higher in the upper SF than in the lower SF (56,900 ± 5,000 vs. 18,500 ± 13,800 ppm, respectively; $t = 5.17$, df = 4.00, $p = 0.007$). No significant difference in upland groundwater pCO_2 was observed between upper and lower SF (10,600 ± 400 vs. 9,200 ± 3,600 ppm, respectively; $t = 0.58$, df = 2.11, $p = 0.57$). Notably, pCO_2 was much higher in riparian groundwater than upland groundwater (elevated 150%–560% across sites).

CO_2 fluxes into and out of the river channel varied over time and space (Figure 3 and Figure S4), but broad patterns were evident. Mean CO_2 emission across all sites was 5.7 g-C m^{-2} d^{-1} (Figure 3b). CO_2 losses from the stream water column were dominated by CO_2 emission since GPP was near zero for all sites, except at ICHE where GPP (3.6 g-C m^{-2} d^{-1}) was almost as large as emission (4.7 g-C m^{-2} d^{-1}). ER was a large CO_2 flux into the river channel at all sites (mean 3.0 g-C m^{-2} d^{-1}). With high ER and low GPP, NEP consistently added CO_2 to all reaches (mean = 2.3 g-C m^{-2} d^{-1}), accounting for 43% of CO_2 emission on average (range = 0–94%); ICHE was the exception, where NEP was near zero because GPP and ER were roughly equal.

The difference between CO_2 emission and NEP, hereafter referred to as "excess CO_2", averaged 3.4 g-C m^{-2} d^{-1} across sites, but was partitioned differently among RIP and TER sources between upper and lower river sites. Five times more CO_2 arrived from the river corridor (RIP, 3.8 g-C m^{-2} d^{-1}) than from the terrestrial uplands (TER, 0.7 g-C m^{-2} d^{-1}) in the upper SF sites (Figure 3b). In contrast, more than 4 times more CO_2 was sourced from TER (3.4 g-C m^{-2} d^{-1}) than RIP (0.8 g-C m^{-2} d^{-1}) at the lower river sites. This arises due to large lateral fluxes of deep aquifer water via karst springs (i.e., TER) at both ICHE and SF2500 (mean = 4.8 g-C m^{-2} d^{-1}). This aquifer lateral flux is more modest in the SF2800 reach, where fewer springs are found, leading to TER estimates similar to those in the upper river (0.7 g-C m^{-2} d^{-1}). Notably, fluxes into and out of the system generally did not balance (the imbalance is labeled "other" in Figure 3b) by about 0.9 g-C m^{-2} d^{-1} on average leaving the water column

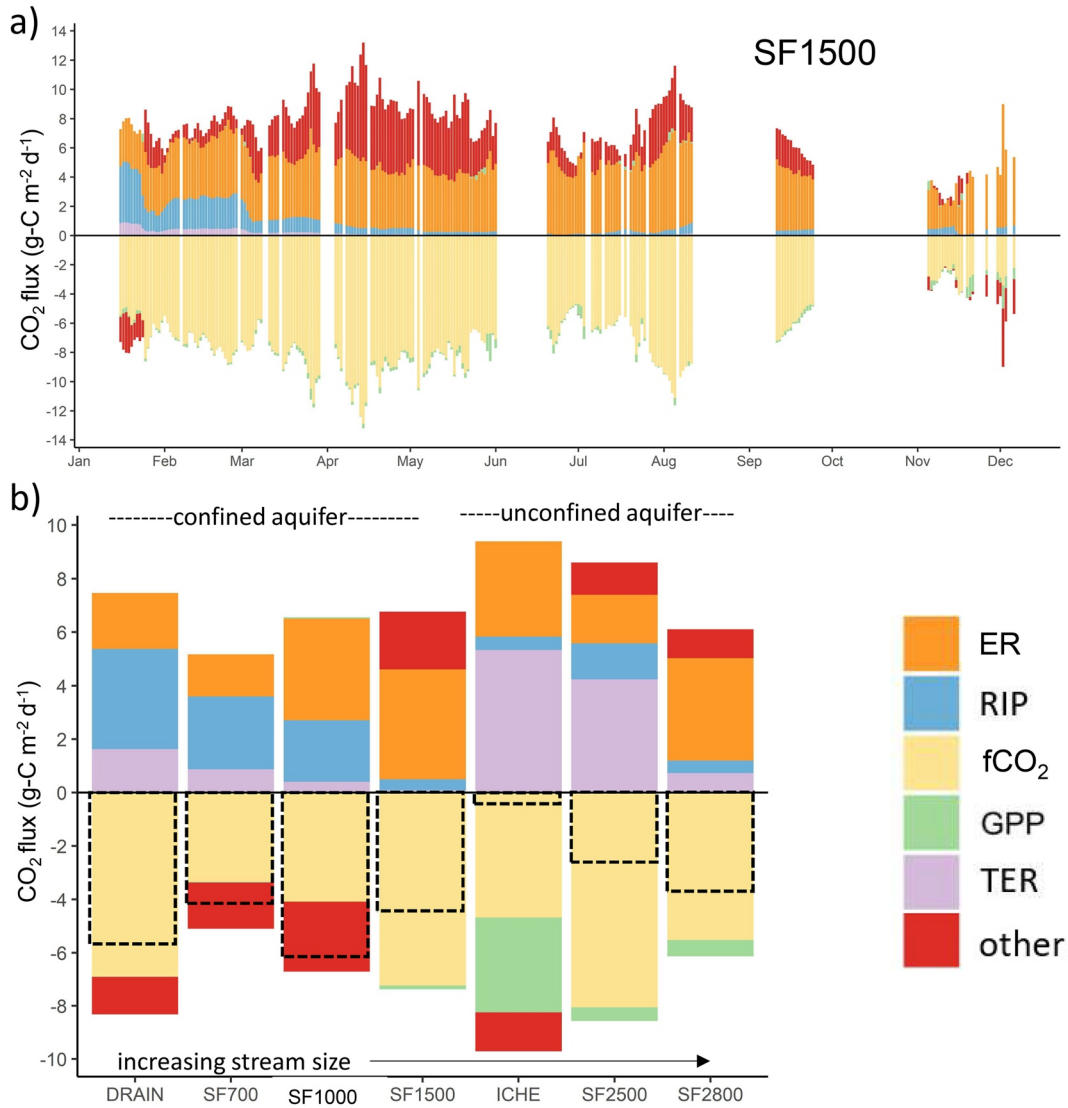

Figure 3. Variation of CO_2 fluxes (a) over time in 2019 at SF1500 (credible intervals are plotted in Figure S4) and (b) for the period of record across the river network (medians fluxes graphed here). CO_2 emission to atmosphere and GPP are considered negative fluxes because CO_2 leaves the river channel. ER (aerobic respiration), RIP (lateral CO_2 from the riparian corridor), and TER (lateral CO_2 from the terrestrial uplands) are considered positive fluxes that bring CO_2 into the river channel. Dashed bars show the portion of fCO_2 that sources from the river corridor.

(i.e., CO_2 sink) in the upper river and 0.3 g-C m^{-2} d^{-1} on average entering the water column (i.e., CO_2 source) in the lower river. Across all sites, TER and RIP each accounted for approximately 34% of CO_2 emission, despite the former occupying far more catchment area. When partitioning sites by hydrogeology, we observe that in the upper SF, TER and RIP accounted for 15% and 49% of CO_2 emission, respectively, while in the lower SF the reverse was true: TER and RIP accounted for 60% and 12% of CO_2 emission, respectively.

Our Monte Carlo simulations of partitioned CO_2 fluxes using observed site means (Table 1) and prior distributions to reflect uncertainties in q_L, $pCO_{2,gw}$, k_{600}, and the respiratory quotient reaffirmed that measured CO_2 fluxes were reasonable (Figures S4, S5). Credible intervals (25%–75%) from posterior distributions mostly aligned with the interquartile ranges of our measured fluxes (Figure S5), justifying our use of observed temporal variation to quantify uncertainties in various component terms to estimate total fluxes.

The aggregate river corridor contribution (i.e., NEP + RIP) accounts for 87% (range 33%–100%) of observed CO_2 emission across nearly all study sites (Figure 3b). The exception is the entirely spring-fed ICHE where dominant

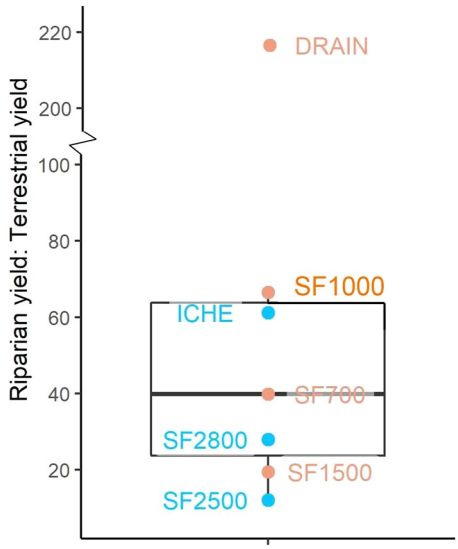

Figure 4. The relative importance of riparian versus terrestrial yields for stream CO_2 emission is summarized as their ratio for all Santa Fe River sites. Brown and blue labeled sites are in the upper (confined aquifer) and lower (unconfined aquifer) basins, respectively.

aquifer contributions of CO_2 (i.e., high TER) and low net metabolic production of CO_2 (i.e., NEP ~ 0) result in the river corridor contributing just 10% of total fCO_2 mass. The river corridor contributes nearly all the CO_2 evaded in the upper basin, but just 37% in the lower river sites, including ICHE.

Across sites, riparian wetlands contributed 40 times more CO_2 per unit area than terrestrial uplands (IQR 24–64 times; Figure 4). This ratio of RIP_{yield} to TER_{yield} was not significantly different between upper and lower basin sites ($t = 1.10$, df = 3.6, $p = 0.34$) despite visual evidence suggesting lower values in the upper basin. Our most headwater site (DRAIN) dramatically underscores the prevailing contrast in CO_2 sources in lower-order locations with a ratio an order of magnitude higher than the rest of the river network (Figure 4). We note that the relative contribution per unit area of riparian versus terrestrial land declines with stream order for the upper basin sites, a finding with potentially important scaling implications. In aggregate, the annual CO_2 yields from terrestrial lands averaged 1.4 g-C m^{-2} yr^{-1}, in stark contrast with the average of 33.1 g-C m^{-2} yr^{-1} from riparian lands. Combining terrestrial and riparian sources, total watershed CO_2 yields are 2.6 g-C m^{-2} yr^{-1}.

4. Discussion

Even though the Santa Fe River sits at the southern extent of the temperate zone (29°N), observed CO_2 emission rates (mean = 5.7 g-C m^{-2} d^{-1}) are better aligned with expectations from the subtropics, where pCO_2 concentrations are generally higher (Butman & Raymond, 2011; Lauerwald et al., 2015). Our observed CO_2 emission rates are nearly double the global mean (3.09 g-C m^{-2} d^{-1}; Hotchkiss et al., 2015) (Figure S6a), but fall within the range reported in the temperate zone (3.70 g-C m^{-2} d^{-1} in Lauerwald et al., 2015; 7.21 g-C m^{-2} d^{-1} in Aufdenkampe et al., 2011) and continental USA (6.49 g-C m^{-2} d^{-1} in Butman & Raymond, 2011). Our comparison with upscaled CO_2 emission rates only provides context, however, since the latter are prone to errors especially if they do not capture sufficient spatial heterogeneity in pCO_2 and k_{600} (Rocher-Ros et al., 2019). Our observed CO_2 emission rates are overall higher—although inconsistently so—than those reported by Khadka et al. (2014) for similar flow regimes on the same river. We attribute these differences to our higher and reach-specific k_{600} values from free-floating dome measurements; Khadka et al. (2014) applied values from anchored domes to the entire river network, and values aligned worse with Raymond equation-derived k_{600} than our measurements. We did not find the expected longitudinal trend of decreasing CO_2 emissions (see Figure S6a; Hotchkiss et al., 2015; Khadka et al., 2014), but the discontinuities along the SF network could be behind the lack of longitudinal pattern.

Given that much of the SF watershed is underlain by carbonate rocks and river water exhibits high alkalinity in the lower network, it seems likely that carbonate buffering serves as an important CO_2 flux in the river network. Indeed, to close the CO_2 mass balance at most sites required an unaccounted for "other" flux (Figure 3 and Figures S4c, S5f), whose sign can indicate CO_2 leaving (negative) or entering (positive) the water. From synoptic dissolved inorganic carbon (DIC) measurements in the SF network (Khadka et al., 2014), CO_2 is likely dissolving carbonate rock in the SF2500 reach as the river emerges from passage underground and comes to equilibrium at the surface, highlighting the potential for dissolution in carbonate regions to damp CO_2 emissions. However, calcite saturation indices calculated through the SF network indicate precipitation of calcite in the lower SF ($SI_{cal} > 0$) and dissolution in the upper SF (Khadka et al., 2014), which corresponds to our observed pattern of the "other" flux. Another pathway in the carbonate buffering system is when dissolved CO_2 ionizes to bicarbonate (and carbonate) as pH increases. In open systems, CO_2 transformed in this manner is replaced by CO_2 from the atmosphere, but in low gradient streams and rivers with low gas exchange rates, ionization occurs much faster than reaeration, so CO_2 is "stored" as bicarbonate. This storage is small when alkalinity is below 1 meq L^{-1} (Stets et al., 2017), which applies in the upper SF. The lower SF has greater potential for CO_2 ionization to bicarbonate (daily rates can be as high as 5.7 g-C m^{-2} d^{-1} at SF2800 which is the reach with highest pH), although mean rates are near zero for all lower SF reaches (Table S2 in Supporting Information S1). Carbonate buffering can work in the opposite direction as well: As CO_2 is lost from the water to the atmosphere via reaeration, it is

replaced by re-equilibration from bicarbonate (Stets et al., 2017). Given relatively high CO_2 emissions from the SF network, this pathway may partly explain the positive "other" fluxes at SF1500 and SF2500 (Figure 3 and Figure S4f). Since we only measured CO_2 concentrations—not those of other DIC species (but see the efforts of Duvert et al., 2019; Wang et al., 2021)—carbonate buffering changes when lateral inflows mix with river water are unknown. The "other" flux reported in this study, arrived at by mass balance, encompasses all those potential carbonate equilibria, but also fluxes due to anaerobic respiration (Bernal et al., 2022) and methane oxidation (Rasilo et al., 2017). Further work will be needed to fully constrain all the overlapping elements of riverine C cycle.

The blackwater metabolic regimes typical in the SF network resulted in high NEP across most sites, making the reactor pathway a major contributor to CO_2 emissions. Compared to a national synthesis of stream metabolism rates (Appling, Hall, et al., 2018; Appling, Read, et al., 2018) with discharge similar to our sites, the SF sites occupy the metabolic extremes. All upper river sites (blackwater streams) had GPP below the 15th percentile (0.14 g-C m^{-2} d^{-1}), while GPP in the spring-fed ICHE was in the 95th percentile. All sites exhibited greater ER than the US median (1.35 g-C m^{-2} d^{-1}), with mean ER across sites above the 90th percentile. Given generally low GPP and high ER, NEP in most SF reaches was a larger source of CO_2 to the air than streams and rivers of comparable size globally (Figure S6b). Moreover, NEP was a larger fraction of CO_2 emission than expected, with the reactor pathway contributing 43% of emissions across the SF, 1.5 times the median value (28%) of lotic CO_2 efflux attributed to internal production more broadly (Hotchkiss et al., 2015). All SF reaches served as venues for net organic matter mineralization except the highly productive ICHE, where large point-scale aquifer inputs of water with very low dissolved organic matter (Duarte et al., 2010) support NEP near zero.

Despite the larger than expected role for in-stream CO_2 production via NEP, the chimney pathway ventilating CO_2 derived from terrestrial OM mineralization and lateral DIC inputs was still a major component of total stream CO_2 emissions. These chimney pathway fluxes varied substantially with both stream size and local hydrogeology. Across this stream network, we did not observe the expected (Hotchkiss et al., 2015) decline in excess CO_2 with stream size (Figure S6c). However, parsing sites between the upper and lower basin revealed that lateral fluxes of CO_2 (i.e., TER + RIP) did indeed decrease with increasing stream size (Figure 3b), a pattern partly driven by declining proportional groundwater inputs (Figure 2b), which implies declining importance of lateral CO_2 fluxes relative to stream CO_2 emission fluxes.

Hydrogeology was the major control on the relative importance of riparian versus terrestrial CO_2 sources to the river. RIP was far higher than TER in the upper basin where the Floridan aquifer is confined, but this situation was reversed in the lower basin where the deep aquifer is unconfined (Figure 3b). This pattern is almost certainly driven by differences in drainage flowpaths. In the karst plain of the lower basin, recharge water carries the CO_2 signal of terrestrial soil respiration to the deep aquifer so that lateral flows to the stream mostly bypass riparian zones, entering the river from deep conduits via discrete spring vents. In the upper basin, by contrast, the surficial aquifer is perched on the Hawthorn Group confining unit, so shallow groundwater water carrying terrestrially derived CO_2 moves laterally through extensive riparian wetlands, entraining significant CO_2 along that flowpath. Given that the SF exhibits these two extremes in aquifer flowpaths, this basin likely also captures extremes in the relative importance of RIP and TER fluxes, suggesting that inferences drawn here from the average of these starkly contrasting settings may be applicable to rivers elsewhere.

The chimney pathway was a major contributor to CO_2 emissions, and our values confirmed that lateral CO_2 fluxes could be estimated by difference (fCO_2–NEP). The total TER + RIP fluxes were similar in magnitude to the lowland Howard River ($Q = 0.16$ m^3 s^{-1}) and partly spring-fed Daly River ($Q = 36$ m^3 s^{-1}) in Australia (1.7 g-C m^{-2} d^{-1} and 6.7 g-C m^{-2} d^{-1}, respectively; Duvert et al., 2019). Measured TER + RIP was 68% of CO_2 emission in the SF, which aligns well with predictions in Hotchkiss et al. (2015) for excess CO_2 (72% from external sources, median 2.22 g-C m^{-2} d^{-1}), but is far higher than has been estimated for southeastern coastal plain region (20%–31%; Butman & Raymond, 2011). We note that mean excess CO_2 (fCO_2–NEP) is 66% of CO_2 emission, which is very similar to our mean summed lateral CO_2 flux (TER + RIP) of 68% of CO_2 emission, suggesting the common practice of equating lateral CO_2 flux with excess CO_2 is a valid approximation. Given the attendant uncertainties in quantifying lateral CO_2 fluxes due to soil pCO_2 heterogeneity (Johnson et al., 2008) and complex lateral flowpaths (Lupon et al., 2019; Rocher-Ros et al., 2019), excess CO_2 may be the easier and more accurate method for estimating the "reactor" versus "chimney" pathways of CO_2 emission, although in streams with higher and discontinuous gas exchange coefficients, capturing fCO_2 heterogeneity along a reach may be difficult.

It is clear that TER was too small to sustain the observed excess CO_2 usually attributed to lateral inorganic C transfer from terrestrial systems. Plausible uncertainty in estimates of groundwater inflow, q_L, could not explain observed excess CO_2 given measured values of groundwater pCO_2 at the upstream edge of the riparian zone (Table 1). Consequently, we estimate that TER contributes only 49% of excess CO_2 across sites, excluding the SF1000 site where excess CO_2 was anomalously low. Without the additional CO_2 sink of carbonate dissolution in many of the sites, CO_2 emission and thus excess CO_2 would be even larger, and TER would be an even smaller fraction of total stream CO_2 emission.

Measured RIP inputs can readily close the clear gap between measured TER and excess CO_2. These findings are similar to those from low-order boreal streams (Leith et al., 2015; Lupon et al., 2019) that emphasize the outsized contribution of riparian zones to stream CO_2 emissions. Despite significant spatial heterogeneity in groundwater pCO_2 estimates (e.g., groundwater pCO_2 up to 90,000 ppm in Amazonia; Johnson et al., 2008), it is clear that the groundwater pCO_2 values of 20,000+ ppm needed to close stream CO_2 budgets based on lateral water fluxes (e.g., Hotchkiss et al., 2015) may be significant overestimates of terrestrially sourced C, and instead better reflect riparian groundwater concentrations (Greenway et al., 2006). This highlights the importance of integrating riparian wetlands into the conceptual model of landscape C mass balances (Abril & Borges, 2019).

The importance of riparian zones in contributing CO_2 to the river channel is further illustrated when lateral CO_2 fluxes are scaled to contributing area. Without disaggregating between RIP and TER contributions, our estimates of 2.6 g-C m^{-2} yr^{-1} compare well to CO_2 catchment yields in Amazonia (Davidson et al., 2010; Lauerwald et al., 2017; Neu et al., 2011) and northern Europe (Dinsmore & Billett, 2008; Leith et al., 2015). Leith et al. (2015) further disaggregated between RIP and TER, and report catchment yields from a boreal, headwater catchment of 3.01 and 1.14 g-C m^{-2} yr^{-1}, respectively. We observed similar TER_{yield} in the SF, but an order of magnitude higher RIP_{yield}, resulting in RIP_{yield} 40 times larger on average than TER_{yield}. The range of modeled lateral CO_2 yields (0–50+ g-C m^{-2} yr^{-1}; Lauerwald et al., 2017) and observed yields across major US river basins (2.5–41.6 g-C m^{-2} yr^{-1}; Butman et al., 2016) suggest that our riparian yields are high (Striegl et al., 2012) but plausible given productive and organic rich riparian ecosystems. While the RIP:TER yield ratio varied substantially among sites (range = 12–216), this variation was not clearly a function of hydrogeologic setting or stream size. Moreover, the ratio always greatly exceeded 1 suggesting riparian areas are important CO_2 subsidy zones for riverine CO_2 ventilation (Abril et al., 2014).

The upper and lower SF sites are end-member rivers with respect to the relative importance of lateral drainage flowpaths, suggesting that estimates from this aggregated catchment-wide study may be broadly applicable and transferrable. Applying the same proportional terrestrial versus riparian C subsidies to streams and rivers elsewhere illustrates the importance of parsing between C sources to help close the continental C budget. Specifically, using our upper and lower SF estimates of mean TER source proportion (15% and 60%, respectively), and the 2.1 Pg-C yr^{-1} of CO_2 outgassed globally from inland waters (Raymond et al., 2013), we estimate that 0.32–1.26 Pg-C yr^{-1} is sourced from lateral CO_2 transferred from terrestrial uplands. If global terrestrial-to-aquatic organic C transfer is 0.75 Pg-C yr^{-1} (Jenerette & Lal, 2005), together CO_2 and organic carbon sourced from terrestrial settings would account for 1.07–2.01 Pg-C yr^{-1}. While this comparison neglects lateral transfer of other species of DIC, this number is already much closer to the 1.9 Pg-C yr^{-1} total lateral C transfer estimated from terrestrial mass balance (Battin et al., 2009; Regnier et al., 2013). That is, updating the inland water pipe model to account for riparian areas as major sources of lateral C transfer (Abril & Borges, 2019), plausibly resolves the large discrepancy between terrestrial and aquatic C mass balances.

The existing conceptual model that parses reactor versus chimney pathways for CO_2 emission focuses on the stream channel as the relevant landscape unit for understanding the "plumbing" of carbon budgets at continental scales. We suggest that the stream corridor, which comprises the stream and the adjacent intermittently flooded lands, is a more salient geographic focus. The combined importance of NEP and RIP (Figure 3b) suggests that despite a modest spatial extent, the river corridor—as clearly distinct from the terrestrial landscape—supplies the overwhelming majority (~87%) of CO_2 eventually evaded by the stream. We further note that the organic C that fuels both reactor and chimney pathways also likely originates in the river corridor. DOC leached from riparian wetlands accounted for 63% of organic C entering a blackwater stream in the southeastern coastal plain (Dosskey & Bertsch, 1994), and studies across biomes have highlighted riparian wetlands as a major source of DOC to streams (Buffam et al., 2011; Ledesma et al., 2015; Strohmeier et al., 2013). Moreover, because of the effective trapping functions of riparian wetlands, most POC contributed to streams is leaf litter and debris from areas

adjacent to the channel (Dosskey & Bertsch, 1994). While the relative magnitudes of different C forms (i.e., CO_2/bicarbonate/DOC/POC) in terrestrial-to-aquatic transfer differs by region (Tank et al., 2018), our results support a revised conceptual model that considers the river corridor loads as the source of most of the C that enters river networks, powering both chimney and reactor pathways that contribute to stream CO_2 emissions.

Data Availability Statement

Data from this study were deposited at Hydroshare via https://www.hydroshare.org/resource/53c0ae4cf09b404fb19a77ed2018e186/.

Acknowledgments
We would like to thank Paul Decker, Kenyon Watkins, and Jemma Thompson for help with fieldwork and data processing, and Ray Thomas for a wizard's introduction to in situ CO_2 sensors. This work was funded by National Science Foundation (DEB 1442140).

References

Abril, G., & Borges, A. V. (2019). Ideas and perspectives: Carbon leaks from flooded land: Do we need to replumb the inland water active pipe? *Biogeosciences*, *16*(3), 769–784. https://doi.org/10.5194/bg-16-769-2019

Abril, G., Martinez, J. M., Artigas, L. F., Moreira-Turcq, P., Benedetti, M. F., Vidal, L., et al. (2014). Amazon River carbon dioxide outgassing fueled by wetlands. *Nature*, *505*(7483), 395–398. https://doi.org/10.1038/nature12797

Appling, A. P., Hall, R. O., Yackulic, C. B., & Arroita, M. (2018). Overcoming equifinality: Leveraging long time series for stream metabolism estimation. *Journal of Geophysical Research: Biogeosciences*, *123*(2), 624–645. https://doi.org/10.1002/2017JG004140

Appling, A. P., Read, J. S., Winslow, L. A., Arroita, M., Bernhardt, E. S., Griffiths, N. A., et al. (2018). Data descriptor: The metabolic regimes of 356 rivers in the United States. *Scientific Data*, *5*, 1–14. https://doi.org/10.1038/sdata.2018.292

Aufdenkampe, A. K., Mayorga, E., Raymond, P. A., Melack, M., Doney, S. C., Doney, C., et al. (2011). Riverine coupling of biogeochemical cycles between land, oceans, and atmosphere. *Frontiers in Ecology and the Environment*, *9*(1), 53–60. https://doi.org/10.1890/100014

Battin, T. J., Luyssaert, S., Kaplan, L. A., Aufdenkampe, A. K., Richter, A., & Tranvik, L. J. (2009). The boundless carbon cycle. *Nature Geoscience*, *2*(9), 598–600. https://doi.org/10.1038/ngeo618

Bernal, S., Cohen, M. J., Ledesma, J. L. J., Kirk, L., Martí, E., & Lupon, A. (2022). Stream metabolism sources a large fraction of carbon dioxide to the atmosphere in two hydrologically contrasting headwater streams. *Limnology & Oceanography*, *67*(12), 1–14. https://doi.org/10.1002/lno.12226

Bosch, D. D., Arnold, J. G., Allen, P. G., Lim, K. J., & Park, Y. S. (2017). Temporal variations in baseflow for the Little River experimental watershed in South Georgia, USA. *Journal of Hydrology: Regional Studies*, *10*, 110–121. https://doi.org/10.1016/j.ejrh.2017.02.002

Buffam, I., Turner, M. G., Desai, A. R., Hanson, P. C., Rusak, J. A., Lottig, N. R., et al. (2011). Integrating aquatic and terrestrial components to construct a complete carbon budget for a north temperate lake district. *Global Change Biology*, *17*(2), 1193–1211. https://doi.org/10.1111/j.1365-2486.2010.02313.x

Burt, T. P., Pinay, G., Matheson, F. E., Haycock, N. E., Butturini, A., Clement, J. C., et al. (2002). Water table fluctuations in the riparian zone: Comparative results from a pan-European experiment. *Journal of Hydrology*, *265*(1–4), 129–148. https://doi.org/10.1016/S0022-1694(02)00102-6

Butman, D., & Raymond, P. A. (2011). Significant efflux of carbon dioxide from streams and rivers in the United States. *Nature Geoscience*, *4*(12), 839–842. https://doi.org/10.1038/ngeo1294

Butman, D., Stackpoole, S., Stets, E., McDonald, C. P., Clow, D. W., & Striegl, R. G. (2016). Aquatic carbon cycling in the conterminous United States and implications for terrestrial carbon accounting. *Proceedings of the National Academy of Sciences of the United States of America*, *113*(1), 58–63. https://doi.org/10.1073/pnas.1512651112

Chen, C. W., Gherini, S. A., Peters, N. E., Murdoch, P. S., Newston, R. M., & Goldstein, R. A. (1984). Hydrologic analyses of acidic and alkaline lakes. *Water Resources Research*, *20*(12), 1875–1882. https://doi.org/10.1029/wr020i012p01875

Chestnut, T. J., & McDowell, W. H. (2000). C and N dynamics in the riparian and hyporheic zones of a tropical stream, Luquillo Mountains, Puerto Rico. *Journal of the North American Benthological Society*, *19*(2), 199–214. https://doi.org/10.2307/1468065

Ciais, P., Borges, A. V., Abril, G., Meybeck, M., Folberth, G., Hauglustaine, D., & Janssens, I. A. (2008). The impact of lateral carbon fluxes on the European carbon balance. *Biogeosciences*, *5*(5), 1259–1271. https://doi.org/10.5194/bg-5-1259-2008

Cirmo, C. P., & McDonnell, J. J. (1997). Linking the hydrologic and biogeochemical controls of nitrogen transport in near-stream zones of temperate-forested catchments: A review. *Journal of Hydrology*, *199*(1–2), 88–120. https://doi.org/10.1016/S0022-1694(96)03286-6

Cole, J. J., & Caraco, N. F. (2001). Carbon in catchments: Connecting terrestrial carbon losses with aquatic metabolism. *Marine and Freshwater Research*, *52*(1), 101–110. https://doi.org/10.1071/mf00084

Cole, J. J., Prairie, Y. T., Caraco, N. F., Mcdowell, W. H., Tranvik, L. J., Striegl, R. G., et al. (2007). Plumbing the global carbon cycle: Integrating inland waters into the terrestrial carbon budget. *Ecosystems*, *10*(1), 171–184. https://doi.org/10.1007/s

Dahl, M., Nilsson, B., Langhoff, J. H., & Refsgaard, J. C. (2007). Review of classification systems and new multi-scale typology of groundwater-surface water interaction. *Journal of Hydrology*, *344*(1–2), 1–16. https://doi.org/10.1016/j.jhydrol.2007.06.027

Davidson, E. A., Figueiredo, R. O., Markewitz, D., & Aufdenkampe, A. K. (2010). Dissolved CO_2 in small catchment streams of eastern Amazonia: A minor pathway of terrestrial carbon loss. *Journal of Geophysical Research*, *115*(4), 1–6. https://doi.org/10.1029/2009JG001202

Devito, K. J., Fitzgerald, D., Hill, A. R., & Aravena, R. (2000). Nitrate dynamics in relation to lithology and hydrologic flow path in a river riparian zone. *Journal of Environmental Quality*, *29*(4), 1075–1084. https://doi.org/10.2134/jeq2000.00472425002900040007x

Dinsmore, K. J., & Billett, M. F. (2008). Continuous measurement and modeling of CO_2 losses from a peatland stream during stormflow events. *Water Resources Research*, *44*(12), 1–11. https://doi.org/10.1029/2008WR007284

Dosskey, M. G., & Bertsch, P. M. (1994). Forest sources and pathways of organic matter transport to a blackwater stream: A hydrologic approach. *Biogeochemistry*, *24*(1), 1–19. https://doi.org/10.1007/BF00001304

Douglas, E. M., Jacobs, J. M., Sumner, D. M., & Ray, R. L. (2009). A comparison of models for estimating potential evapotranspiration for Florida land cover types. *Journal of Hydrology*, *373*(3–4), 366–376. https://doi.org/10.1016/j.jhydrol.2009.04.029

Drake, T. W., Raymond, P. A., & Spencer, R. G. M. (2018). Terrestrial carbon inputs to inland waters: A current synthesis of estimates and uncertainty. *Limnology and Oceanography Letters*, *3*(3), 132–142. https://doi.org/10.1002/lol2.10055

Duarte, C. M., Prairie, Y. T., Frazer, T. K., Hoyer, M. V., Notestein, S. K., Martínez, R., et al. (2010). Rapid accretion of dissolved organic carbon in the springs of Florida: The most organic-poor natural waters. *Biogeosciences*, *7*(12), 4051–4057. https://doi.org/10.5194/bg-7-4051-2010

Duvert, C., Bossa, M., Tyler, K. J., Wynn, J. G., Munksgaard, N. C., Bird, M. I., et al. (2019). Groundwater-derived DIC and carbonate buffering enhance fluvial CO_2 evasion in two Australian tropical rivers. *Journal of Geophysical Research: Biogeosciences*, *124*(2), 312–327. https://doi.org/10.1029/2018JG004912

Eckhardt, K. (2008). A comparison of baseflow indices, which were calculated with seven different baseflow separation methods. *Journal of Hydrology*, *352*(1–2), 168–173. https://doi.org/10.1016/j.jhydrol.2008.01.005

Fisher, S. G., Grimm, N. B., Martí, E., Holmes, R. M., & Jones, J. B. (1998). Material spiraling in stream corridors: A telescoping ecosystem model. *Ecosystems*, *1*(1), 19–34. https://doi.org/10.1007/s100219900003

Fisher, S. G., Sponseller, R. A., & Heffernan, J. B. (2004). Horizons in stream biogeochemistry: Flowpaths to progress. *Ecology*, *85*(9), 2369–2379. https://doi.org/10.1890/03-0244

Florida Natural Areas Inventory. (1990). Guide to the natural communities of Florida.

Fuka, D., Walter, M., Archibald, J., Steenhuis, T., & Easton, Z. (2018). A community modeling foundation for eco-hydrology.

Gómez-Gener, L., Rocher-Ros, G., Battin, T., Cohen, M. J., Dalmagro, H. J., Dinsmore, K. J., et al. (2021). Global carbon dioxide efflux from rivers enhanced by high nocturnal emissions. *Nature Geoscience*, *14*(5), 289–294. https://doi.org/10.1038/s41561-021-00722-3

Greenway, H., Armstrong, W., & Colmer, T. D. (2006). Conditions leading to high CO_2 (>5 kPa) in waterlogged-flooded soils and possible effects on root growth and metabolism. *Annals of Botany*, *98*(1), 9–32. https://doi.org/10.1093/aob/mcl076

Hall, R. O., & Tank, J. L. (2005). Correcting whole-stream estimates of metabolism for groundwater input. *Limnology and Oceanography: Methods*, *3*(4), 222–229. https://doi.org/10.4319/lom.2005.3.222

Harvey, J. W., & Gooseff, M. (2015). River corridor science: Hydrologic exchange and ecological consequences from bedforms to basins. *Water Resources Research*, *51*(9), 6893–6922. https://doi.org/10.1002/2015WR017617.Received

Hedin, L. O., Von Fischer, J. C., Ostrom, N. E., Kennedy, B. P., Brown, M. G., & Philip Robertson, G. (1998). Thermodynamic constraints on nitrogen transformations and other biogeochemical processes at soil-stream interfaces. *Ecology*, *79*(2), 684–703. https://doi.org/10.1890/0012-9658(1998)079[0684:TCONAO]2.0.CO;2

Hensley, R. T., Cohen, M. J., & Korhnak, L. V. (2015). Hydraulic effects of nitrogen removal in a tidal spring-fed river. *Water Resources Research*, *51*(3), 1443–1456. https://doi.org/10.1002/2015WR017200.A

Hensley, R. T., Decker, P. H., Flinders, C., McLaughlin, D., Schilling, E., & Cohen, M. J. (2020). Fertilization has negligible effects on nutrient export and stream biota in two North Florida forested watersheds. *Forest Ecology and Management*, *465*(March), 118096. https://doi.org/10.1016/j.foreco.2020.118096

Hensley, R. T., Kirk, L., Spangler, M., Gooseff, M. N., & Cohen, M. J. (2019). Flow extremes as spatiotemporal control points on river solute fluxes and metabolism. *Journal of Geophysical Research: Biogeosciences*, *124*(3), 537–555. https://doi.org/10.1029/2018JG004738

Hooper, R. P., Aulenbach, B. T., Burns, D., McDonnel, J. J., & Freer, J. (1998). *Riparian control of stream-water chemistry: Implications for hydrochemical basin models* (Vol. 248, pp. 451–458). HIAHS publications-series of proceedings and reports-Internternational Association of Soc Hydrological Sciences.

Hotchkiss, E. R., Hall, R. O., Jr., Sponseller, R. A., Butman, D., Klaminder, J., Laudon, H., et al. (2015). Sources of and processes controlling CO_2 emissions change with the size of streams and rivers. *Nature Geoscience*, *8*(9), 696–699. https://doi.org/10.1038/ngeo2507

Jenerette, G. D., & Lal, R. (2005). Hydrologic sources of carbon cycling uncertainty throughout the terrestrial-aquatic continuum. *Global Change Biology*, *11*(11), 1873–1882. https://doi.org/10.1111/j.1365-2486.2005.01021.x

Jin, J., Zimmerman, A. R., Martin, J. B., & Khadka, M. B. (2015). Spatiotemporal variations in carbon dynamics during a low flow period in a carbonate karst watershed: Santa Fe River, Florida, USA. *Biogeochemistry*, *122*(1), 131–150. https://doi.org/10.1007/s10533-014-0035-6

Johnson, M. S., Lehmann, J., Couto, E. G., Filho, J. P. N., & Riha, S. J. (2006). DOC and DIC in flowpaths of Amazonian headwater catchments with hydrologically contrasting soils. *Biogeochemistry*, *81*(1), 45–57. https://doi.org/10.1007/s10533-006-9029-3

Johnson, M. S., Lehmann, J., Riha, S. J., Krusche, A. V., Richey, J. E., Ometto, J. P. H. B., & Guimara, E. (2008). CO_2 efflux from Amazonian headwater streams represents a significant fate for deep soil respiration. *Geophysical Research Letters*, *35*(17), 1–5. https://doi.org/10.1029/2008GL034619

Junk, W. J. (1989). The flood pulse concept in river-floodplain systems. In D. P. Dodge (Ed.), *Proceedings of the International large river symposium* (Vol. 106, pp. 110–127). Canadian Special Publications in Fisheries and Aquatic Sciences. https://doi.org/10.1007/BF02564079

Kalbus, E., Reinstorf, F., & Schirmer, M. (2006). Measuring methods for groundwater-surface water interactions: A review. *Hydrology and Earth System Sciences*, *10*(6), 873–887. https://doi.org/10.5194/hess-10-873-2006

Khadka, M. B., Martin, J. B., & Jin, J. (2014). Transport of dissolved carbon and CO_2 degassing from a river system in a mixed silicate and carbonate catchment. *Journal of Hydrology*, *513*, 391–402. https://doi.org/10.1016/j.jhydrol.2014.03.070

Khadka, M. B., Martin, J. B., & Kurz, M. J. (2017). Synoptic estimates of diffuse groundwater seepage to a spring-fed karst river at high spatial resolution using an automated radon measurement technique. *Journal of Hydrology*, *544*, 86–96. https://doi.org/10.1016/j.jhydrol.2016.11.013

Kirk, L., & Cohen, M. J. (2022). River corridor sources dominate CO_2 emissions from a lowland river network. *HydroShare*. https://doi.org/10.4211/hs.53c0ae4cf09b404fb19a77ed2018e186

Kirk, L., Hensley, R. T., Savoy, P., Heffernan, J. B., & Cohen, M. J. (2020). Estimating benthic light regimes improves predictions of primary production and constrains light-use efficiency in streams and rivers. *Ecosystems*, *24*(4), 825–839. https://doi.org/10.1007/s10021-020-00552-1

Kurz, M. J., Martin, J. B., Cohen, M. J., & Hensley, R. T. (2015). Diffusion and seepage-driven element fluxes from the hyporheic zone of a Karst river. *Freshwater Science*, *34*(1), 206–221. https://doi.org/10.1086/679654

Lamberti, G. A., & Hauer, R. (2017). Ecosystem processes. In *Methods in stream ecology* (3rd ed.). Academic Press.

Lauerwald, R., Laruelle, G. G., Hartmann, J., Ciais, P., & Regnier, P. (2015). Spatial patterns in CO_2 evasion from the global river network. *Global Biogeochemical Cycles*, *29*(5), 534–554. https://doi.org/10.1111/1462-2920.13280

Lauerwald, R., Regnier, P., Camino-Serrano, M., Guenet, B., Guimberteau, M., Ducharne, A., et al. (2017). ORCHILEAK (revision 3875): A new model branch to simulate carbon transfers along the terrestrial-aquatic continuum of the Amazon basin. *Geoscientific Model Development*, *10*(10), 3821–3859. https://doi.org/10.5194/gmd-10-3821-2017

Leach, J., Lidberg, W., Kuglerova, L., Peralta-Tapia, A., Agren, A., & Laudon, H. (2017). Evaluating topography-based predictions of shallow lateral groundwater discharge zones for a boreal lake-stream system. *Water Resources Research*, *53*(7), 5998–6017. https://doi.org/10.1002/2016WR019804.Received

Ledesma, J. L. J., Grabs, T., Bishop, K. H., Schiff, S. L., & Köhler, S. J. (2015). Potential for long-term transfer of dissolved organic carbon from riparian zones to streams in boreal catchments. *Global Change Biology*, *21*(8), 2963–2979. https://doi.org/10.1111/gcb.12872

Ledesma, J. L. J., Kothawala, D. N., Bastviken, D., Maehder, S., Grabs, T., & Futter, M. N. (2018). Stream dissolved organic matter composition reflects the riparian zone, not upslope soils in boreal forest headwaters. *Water Resources Research*, *54*(6), 3896–3912. https://doi.org/10.1029/2017WR021793

Leith, F. I., Dinsmore, K. J., Wallin, M. B., Billett, M. F., Heal, K. V., Laudon, H., et al. (2015). Carbon dioxide transport across the hillslope-riparian-stream continuum in a boreal headwater catchment. *Biogeosciences*, *12*(6), 1881–1902. https://doi.org/10.5194/bg-12-1881-2015

Leopold, L. B., & Maddock, T. (1953). The hydraulic geometry of stream channels and some physiographic implications. USGS Professional Paper 252.

Liu, S., Kuhn, C., Amatulli, G., Aho, K., Butman, D. E., & Allen, G. H. (2022). The importance of hydrology in routing terrestrial carbon to the atmosphere via global streams and rivers (pp. 1–9). https://doi.org/10.1073/pnas.2106322119/-/DCSupplemental.Published

Lupon, A., Denfeld, B. A., Laudon, H., Leach, J., Karlsson, J., & Sponseller, R. A. (2019). Groundwater inflows control patterns and sources of greenhouse gas emissions from streams. *Limnology & Oceanography*, *64*(4), 1–13. https://doi.org/10.1002/lno.11134

Maître, V., Cosandey, A. C., Desagher, E., & Parriaux, A. (2003). Effectiveness of groundwater nitrate removal in a river riparian area: The importance of hydrogeological conditions. *Journal of Hydrology*, *278*(1–4), 76–93. https://doi.org/10.1016/S0022-1694(03)00134-3

Mayorga, E., Aufdenkampe, A. K., Masiello, C. A., Krusche, A. V., Hedges, J. I., Quay, P. D., et al. (2005). Young organic matter as a source of carbon dioxide outgassing from Amazonian rivers. *Nature*, *436*(July), 358–341. https://doi.org/10.1038/nature03880

Mitra, S., Wassmann, R., & Vlek, P. L. G. (2005). An appraisal of global wetland area and its organic carbon stock. *Current Science*, *88*(1), 25–35.

Mulholland, P. J. (1993). Hydrometric and stream chemistry evidence of three storm flowpaths in Walker Branch Watershed. *Journal of Hydrology*, *151*(2–4), 291–316. https://doi.org/10.1016/0022-1694(93)90240-a

Naiman, R. J., & Décamps, H. (1997). The ecology of interfaces: Riparian zones. *Annual Review of Ecology and Systematics*, *28*(102), 621–658. https://doi.org/10.1146/annurev.ecolsys.28.1.621

Nathan, R. J., & McMahon, T. A. (1990). Evaluation of automated techniques for base flow and recession analyses. *Water Resources Research*, *26*(7), 1465–1473. https://doi.org/10.1029/WR026i007p01465

Neu, V., Neill, C., & Krusche, A. V. (2011). Gaseous and fluvial carbon export from an Amazon forest watershed. *Biogeochemistry*, *105*(1), 133–147. https://doi.org/10.1007/s10533-011-9581-3

Odum, H. T. (1956). Primary production in flowing waters. *Limnology & Oceanography*, *1*(2), 102–117. https://doi.org/10.4319/lo.1956.1.2.0102

Odum, H. T. (1957). Trophic structure and productivity of silver springs. *Ecological Monographs*, *27*(1), 55–112. https://doi.org/10.2307/1948571

Ohrui, K., & Mitchell, M. J. (1999). Hydrological flow paths controlling stream chemistry in Japanese forested watersheds. *Hydrological Processes*, *13*(6), 877–888. https://doi.org/10.1002/(SICI)1099-1085(19990430)13:6<877::AID-HYP762>3.0.CO;2-E

Puckett, L. J., Cowdery, T. K., McMahon, P. B., Tornes, L. H., & Stoner, J. D. (2002). Using chemical, hydrologic, and age dating analysis to delineate redox processes and flow paths in the riparian zone of a glacial outwash aquifer-stream system. *Water Resources Research*, *38*(8), 9-1–9-20. https://doi.org/10.1029/2001wr000396

Rasilo, T., Hutchins, R. H. S., Ruiz-González, C., & del Giorgio, P. A. (2017). Transport and transformation of soil-derived CO_2, CH_4 and DOC sustain CO_2 supersaturation in small boreal streams. *Science of the Total Environment*, *579*, 902–912. https://doi.org/10.1016/j.scitotenv.2016.10.187

Raymond, P. A., Hartmann, J., Lauerwald, R., Sobek, S., McDonald, C., Hoover, M., et al. (2013). Global carbon dioxide emissions from inland waters. *Nature*, *503*(7476), 355–359. https://doi.org/10.1038/nature12760

Raymond, P. A., Saiers, J. E., & Sobczak, W. V. (2016). Hydrological and biogeochemical controls on watershed dissolved organic matter transport: Pulse-shunt concept. *Ecology*, *97*(1), 5–16. https://doi.org/10.1890/14-1684.1

Raymond, P. A., Zappa, C. J., Butman, D., Bott, T. L., Potter, J., Mulholland, P., et al. (2012). Scaling the gas transfer velocity and hydraulic geometry in streams and small rivers. *Limnology and Oceanography: Fluids and Environments*, *2*(1), 41–53. https://doi.org/10.1215/21573689-1597669

Regnier, P., Friedlingstein, P., Ciais, P., Mackenzie, F. T., Gruber, N., Janssens, I. A., et al. (2013). Anthropogenic perturbation of the carbon fluxes from land to ocean. *Nature Geoscience*, *6*(8), 597–607. https://doi.org/10.1038/ngeo1830

Regnier, P., Resplandy, L., Najjar, R. G., & Ciais, P. (2022). The land-to-ocean loops of the global carbon cycle. *Nature*, *603*(March), 401–410. https://doi.org/10.1038/s41586-021-04339-9

Rocher-Ros, G., Sponseller, R. A., Lidberg, W., Mörth, C., & Giesler, R. (2019). Landscape process domains drive patterns of CO_2 evasion from river networks. *Limnology and Oceanography Letters*, *4*(4), 87–95. https://doi.org/10.1002/lol2.10108

Saccardi, B., & Winnick, M. (2021). Improving predictions of stream CO_2 concentrations and fluxes using a stream network model: A case study in the East River Watershed, CO, USA. *Global Biogeochemical Cycles*, *35*(12). https://doi.org/10.1029/2021GB006972

Siemens, J., & Villarreal, L. P. (2003). The European carbon budget: A gap. *Science*, *302*(5651), 1681. https://doi.org/10.1126/science.302.5651.1677b

Smith, F. L., & Harvey, A. H. (2007). Avoid common pitfalls when using Henry' s law. *Environmental Management*, *103*(September), 33–39.

Stets, E. G., Butman, D., McDonald, C. P., Stackpoole, S. M., DeGrandpre, M. D., & Striegl, R. G. (2017). Carbonate buffering and metabolic controls on carbon dioxide in rivers. *Global Biogeochemical Cycles*, *31*(4), 663–677. https://doi.org/10.1002/2016GB005578

Striegl, R. G., Dornblaser, M. M., McDonald, C. P., Rover, J. R., & Stets, E. G. (2012). Carbon dioxide and methane emissions from the Yukon River system. *Global Biogeochemical Cycles*, *26*(4). https://doi.org/10.1029/2012GB004306

Strohmeier, S., Knorr, K. H., Reichert, M., Frei, S., Fleckenstein, J. H., Peiffer, S., & Matzner, E. (2013). Concentrations and fluxes of dissolved organic carbon in runoff from a forested catchment: Insights from high frequency measurements. *Biogeosciences*, *10*(2), 905–916. https://doi.org/10.5194/bg-10-905-2013

Suwanee River Water Management District. (2007). MFL establishment for the upper Santa Fe River. Retrieved from http://www.mysuwanneeriver.com/documentcenter/view/133

Suwanee River Water Management District. (2019). Minimum flows and minimum water levels re-evaluation for the Lower Santa Fe and Ichetucknee Rivers and priority springs - Draft.

Tank, S. E., Fellman, J. B., Hood, E., & Kritzberg, E. S. (2018). Beyond respiration: Controls on lateral carbon fluxes across the terrestrial-aquatic interface. *Limnology and Oceanography Letters*, *3*(3), 76–88. https://doi.org/10.1002/lol2.10065

Vidon, P., Allan, C., Burns, D., Duval, T. P., Gurwick, N., Inamdar, S., et al. (2010). Hot spots and hot moments in riparian zones: Potential for improved water quality management. *Journal of the American Water Resources Association*, *46*(2), 278–298. https://doi.org/10.1111/j.1752-1688.2010.00420.x

Wang, C., Xie, Y., Liu, S., Mccallum, J. L., Li, Q., & Wu, J. (2021). Effects of diffuse groundwater discharge, internal metabolism and carbonate buffering on headwater stream CO_2 evasion. *Science of the Total Environment*, *777*, 146230. https://doi.org/10.1016/j.scitotenv.2021.146230

References From the Supporting Information

Dahm, C. N., & Valett, H. M. (1996). Hyporheic zones. In R. Hauer, & G. A. Lamberti (Eds.), *Methods in stream ecology* (p. 673). Academic Press.

Godsey, S. E., Kirchner, J. W., & Clow, D. W. (2009). Concentration-discharge relationships reflect chemostatic characteristics of US catchments. *Hydrological Processes*, *23*(13), 1844–1864. https://doi.org/10.1002/hyp

Hoagland, B., Russo, T. A., Brantley, S. L., Hill, L., Kaye, J., & Forsythe, B. (2017). Relationships in a headwater sandstone stream. *Water Resources Research*, *53*(6), 4643–4667. https://doi.org/10.1002/2016WR019717.Received

Hvorslev, M. J. (1951). Time lag and soil permeability in ground-water observations. *US Army Corps of Engineers Waterways Experimental Station Bulletin*, *36*, 1–50.

Jin, J., Zimmerman, A. R., Moore, P. J., & Martin, J. B. (2014). Organic and inorganic carbon dynamics in a karst aquifer: Santa Fe River Sink-Rise system, North Florida, USA. *Journal of Geophysical Research: Biogeosciences*, *119*(3), 340–357. https://doi.org/10.1002/2013JG002350.Received

Musolff, A., Fleckenstein, J. H., Rao, P. S. C., & Jawitz, J. W. (2017). Emergent archetype patterns of coupled hydrologic and biogeochemical responses in catchments. *Geophysical Research Letters*, *44*(9), 4143–4151. https://doi.org/10.1002/2017GL072630

Musolff, A., Schmidt, C., Selle, B., & Fleckenstein, J. H. (2015). Catchment controls on solute export. *Advances in Water Resources*, *86*, 133–146. https://doi.org/10.1016/j.advwatres.2015.09.026

Pierrot, D., Lewis, E., Wallace, D. W. R. (2006). *MS excel program developed for CO_2 system calculations. ORNL/CDIAC-105a. Carbon dioxide information analysis center*. Oak Ridge National Laboratory, U.S. Department of Energy. https://doi.org/10.3334/CDIAC/otg.CO2SYS_XLS_CDIAC105a